**Applicability of magnetic force models for multi-stable energy harvesters**

**Ying Zhang[1], Wei-Hsin Liao[2], Chris Bowen[3], Wei Wang[4], Junyi Cao[1,*]**

[1] Key Laboratory of Education Ministry for Modern Design and Rotor-Bearing System,

School of Mechanical Engineering, Xi'an Jiaotong University, Xi'an, 710049, China

[2] Department of Mechanical and Automation Engineering, The Chinese University of Hong Kong,

Shatin, N.T., Hong Kong, China

[3] Department of Mechanical Engineering, University of Bath, BA2 7AY Bath, UK

[4] School of Mechanics and Safety Engineering, Zhengzhou University, Zhengzhou, 450001, China

[*]Corresponding author e-mail: caojy@mail.xjtu.edu.cn

**Abstract**

Multi-stable piezoelectric energy harvesters have been exploited to enhance performance for extracting ambient vibrational energy from a broadband energy source. Since magnetic force plays a significant role in enhancing the dynamic behavior of harvesters, it is necessary to model and understand the significant influencing of structural parameters on magnetic force. Recently, several theoretical modeling methods, including magnetic dipole, improved dipole, magnetic current and magnetic charge models, have been developed to calculate the magnetic force in multi-stable energy harvesters. However, the influence of structural parameters and magnet dimensions on the accuracy of magnetic force calculation for these methods has not been analyzed. Therefore, it is necessary to investigate the applicability of these methods under a range of operating conditions. New insights into the accuracy and application constraints of these methods are presented in this paper to calculate the impact of magnetic force on multi-stable energy harvesters. From the theoretical derivation of models and numerical results obtained, a quantitative assessment of errors under different structural parameters and magnet sizes is presented and compared to evaluate the application constraints. Moreover, experimental measurements are performed to verify the applicability of these modeling methods for bi-stable and tri-stable energy harvesters with different structural parameters.

**Keywords**: Multi-stable energy harvester; magnetic force; nonlinearity; theoretical modeling

## 1. Introduction

A number of researchers have devoted significant effort to enhancing the performance of traditional energy harvesters (Cottone et al., 2009; Fang et al., 2020a; Yang et al., 2018; Zhao et al., 2019a). The nonlinear energy harvester has received much attention since its stiffness can be adjusted to broaden the resonant frequency for performance enhancement (Barton et al., 2010; Fang et al., 2020b; Fang et al., 2020c; Gammaitoni et al., 2009; Tang and Yang, 2012; Zhao et al., 2018; Zou et al., 2017). There are two main methods to achieve nonlinearity, including the *mechanical* method and the *magnetic* coupled method. The mechanical method aims to generate the complex buckling of the structures, but this is difficult to accurately design and control ( Arrieta et al., 2010; Leland and Wright, 2006). However, the magnetic coupled method is preferable and is achieved by employing a magnetic force which can lead to a compact device structure and can be easily adjusted.

It has been demonstrated that magnetic coupled nonlinear energy harvesters outperform their linear counterparts (Stanton et al., 2009). Among the different types of configurations, multi-stable piezoelectric energy harvesters have been widely developed and investigated as a result of their favorable dynamic characteristics (Kim and Seok, 2014; Lai et al., 2019; Wang et al., 2018a; Zhou et al., 2014). Cottone et al. (2009) investigated the nonlinear characteristics of a bi-stable energy harvester which was achieved using a piezoelectric inverted pendulum, whose response was better than the linear oscillators under stochastic excitations. Erturk et al. (2009) designed a bi-stable piezoelectric energy harvester to scavenge vibrational energy sources based on a nonlinear magnetoelastic strange attractor (Moon and Holmes, 1979), which demonstrated that the voltage amplitude of this structure can achieve a 200% increase under a harmonic excitation. The effectiveness of the bi-stable device proposed by Erturk et al. (2009) under the random excitations was also verified by Litak et al. (2010). In addition, He and Daqaq (2016) investigated the optimal electric load of a mono-stable energy harvester under white noise excitations. Koszewnik et al. (2022) presented the optimization process of magnetic coupled piezoelectric harvesters for performance enhancement by choosing optimal parameters. The bi-stable magneto-piezoelastic absorber and bi-stable PZT-based absorber were exploited for simultaneous energy harvesting and vibration mitigation (Rezaei et al., 2021; Rezaei et al., 2022). In order to further improve the performance, a tri-stable piezoelectric energy harvester that was formed by replacing the fixed external magnets with rotatable external magnets was proposed, which led to improved performance since it can pass through the potential energy wells more easily than a bi-stable energy harvester with deeper potential wells (Zhou et al., 2013; Zhou et al., 2014) . Rezaei and Talebitooti (2022) investigated the performance of tri-stable magneto-piezoelastic absorber for energy harvesting and vibration suppression. To optimize the output performance of tri-stable energy harvesters, Cao et al. (2015) analyzed the effects of potential well depth on the energy harvesting performance, revealing that a shallower potential well depth can lead to a higher broadband performance under low frequency ambient vibrations. However, although the relationship between the nonlinear restoring force and the voltage response of the multi-stable energy harvesters has been investigated in these works, the method to design the nonlinear restoring force has yet to be discussed in detail. Therefore, in order to understand the significant influencing of the structural parameters on the nonlinear restoring force, it is essential to theoretically model the restoring force and its nonlinear characteristics. While the magnetic force plays a significant role in the nonlinearity of restoring force, it is difficult to calculate since it is highly sensitive to the spatial positions of the magnets.

There are three main approaches to acquire the magnetic force of multi-stable energy harvesters; these include the finite element method, experimental measurement, and theoretical modeling. The finite element method is usually achieved by a variety of commercial software tools. Upadrashta and Yang (2015) used the finite element modeling method to model nonlinear harvesters and calculate the magnetic force by using a nonlinear spring element available in ANSYS, which could accurately analyze the behavior of nonlinear harvesters with magnetic interaction. However, the accuracy of finite element method relies heavily on the time-consuming refinement of meshing. In addition, the experimental measurement aims to fit an expression of magnetic force from measured data. Zhou et al. (2014) applied a polynomial to fit the nonlinear restoring force to numerically verify the performance of both bi-stable and tri-stable energy harvesters. Abdelmoula et al. (2017) compared the accuracy between different order polynomials to fit the nonlinear magnetic force, and showed that the fifth order and seventh order polynomials can achieve high accuracy. Although this method can achieve an accurate expression of magnetic force, it requires a new analysis if any of the operational parameters change.

In addition to finite element method and experimental measurement, the theoretical modeling method has attracted significant attention. Several popular methods include the magnetic dipole method, improved dipole method, magnetic current method, and magnetic charge method. Firstly, the magnetic dipole method was presented by Yung et al. (1998) which regards the magnet as a magnetic dipole located in the geometric center of the magnet and was widely used in the magnetic force calculation for energy harvesting (Lai et al., 2019; Li et al., 2016; Wang et al., 2018a; Zhao et al., 2019b). Zhao et al. (2019b) employed the magnetic dipole method to analyze the change of magnetic force between the rotor magnet and the external magnet for a water-proof magnetically coupled hybrid wind energy harvester. Li et al. (2016) derived the magnetic repulsive force of the tri-stable piezoelectric energy harvester based on the magnetic dipole method. Secondly, based on magnetic dipole method, an improved dipole method was developed to calculate the magnetic force for a tri-stable piezoelectric energy harvester (Wang et al., 2019; Wang et al., 2020). The improved dipole method was utilized to calculate the magnetic force for investigating the performance of simultaneous energy harvesting and vibration isolation of bi-stable and tri-stable absorber (Rezaei et al., 2021; Rezaei et al., 2022; Rezaei and Talebitooti, 2022). Thirdly, based on the research by Agashe and Arnold (2008), Gao et al. (2016) and Leng et al. (2017) applied the magnetic current method to calculate the magnetic force for the bi-stable and tri-stable piezoelectric energy harvesters. Finally, a magnetic charge method was developed from magnetic potential theory to calculate the magnetic force for cubic magnets (Akoun and Yonnet, 1984; Charpentier and Lemarquand, 1999). Fu and Yeatman (2017) analyzed the change of magnetic force when the external magnet rotates for low frequency nonlinear energy harvester. Then, Zhang et al. (2021) proposed a rotational magnetic charge method to calculate the magnetic force for a range of structural parameters.

However, the influence of structural parameters and the magnets dimensions on the accuracy of magnetic force calculation for the above methods has not been analyzed. As a result, the applicability and the application constraints should be deeply investigated. This paper therefore presents new insights into the accuracy and application constraints of magnetic dipole, improved dipole, magnetic current and magnetic charge methods to calculate the magnetic force of multi-stable energy harvesters, predominately for bi-stable piezoelectric energy harvesters (BPEH) and tri-stable piezoelectric energy harvesters (TPEH). The applicability for these modeling methods is clarified based on finite element analysis and theoretical evaluations of the different methods. Moreover, experiments under different conditions are carried out to demonstrate the modeling applicability in calculating the magnetic force for different structural parameters. This paper is organized as follows: Sect. 2 provides the theoretical modeling process of magnetic force for different modeling methods for multi-stable piezoelectric energy harvesters. The applicability and the detailed application constraints are then investigated based on the numerical simulation in Sect. 3. In Sect. 4, experimental investigation of modeling magnetic force methods is carried out. The conclusions are drawn in Sect. 5.

## 2. Models of multi-stable piezoelectric energy harvesters

### 2.1 Multi-stable piezoelectric energy harvesters

The cantilever beam structure is a popular form of multi-stable piezoelectric energy harvesters (Erturk et al., 2009). This kind of structure is achieved by employing one or more external magnets to generate the nonlinear magnetic force on the tip magnet of cantilever beam. Therefore, the restoring force becomes nonlinear, and its stiffness changes for different displacements. Since the superior performance of such structures provides a potential alternative for a sustainable energy supply, many different configurations based on this cantilever beam structure have been developed for performance enhancement.

Multi-stable piezoelectric energy harvesters predominantly include bi-stable (Cottone et al., 2009;

Erturk et al., 2009; Masana and Daqaq, 2011; Stanton et al., 2010) and tri-stable (Zhou et al., 2013; Zhou et al., 2014) systems, and asymmetric configurations (Harne and Wang, 2014; He and Daqaq, 2014; Wang et al., 2018b). In order to improve the efficiency, these works have concentrated on the influence of potential well shape on dynamic responses, such as bifurcations, chaos and inter-well motion. Therefore, the design of the potential well plays a significant role in performance enhancement, and it can be understood and optimized by modeling magnetic restoring force theoretically.

Figure 1 depicts a BPEH, which includes piezoelectric ceramics, cantilever beam, tip magnet and external magnet. The piezoelectric ceramics are located close to the root of cantilever beam to generate the electric energy according to the direct piezoelectric effect. The tip magnet is located at the free end of the cantilever beam, and is subjected to the magnetic force from the external magnet. The restoring force of a multi-stable energy harvester is nonlinear, with more than one balancing points. The BPEH has two stable balancing points and one unstable balancing point, while the TPEH contains three stable balancing points and two unstable balancing points. Therefore, stable balancing points can produce the corresponding potential wells. If the cantilever beam oscillates and crosses different potential wells, the displacement of cantilever beam will be large, thus maintaining a high-energy orbit and providing more electricity.

Since the displacement of cantilever beam mainly comes from the first resonant mode, the governing equations of multi-stable energy harvesters based on the Hamilton principle and Euler-Bernoulli beam theory are given by (Erturk, 2012; Stanton et al., 2010)

$$\begin{cases} M\ddot{y}(t) + C_c\dot{y}(t) + Ky(t) + F_m - \xi v(t) = F(t) \\ C_p\dot{v}(t) + v(t)(R_l)^{-1} + \xi\dot{y}(t) = 0 \end{cases} \tag{1}$$

where

$M$ the equivalent mass of multi-stable energy harvester

$C_c$ the equivalent damping of multi-stable energy harvester

$K$ the equivalent stiffness of multi-stable energy harvester

$\xi$ the electromechanical coupling coefficient

$C_p$ the equivalent capacitance of the piezoelectric ceramic

$R_l$ the load resistance of external circuit

$v(t)$ the voltage generated by the piezoelectric ceramic

$y(t)$ the transverse displacement of the cantilever beam

$F(t)$ the external excitation

$F_m$ the magnetic force.

It should be noted that the combination of the elastic force from the cantilever beam and the magnetic force from external magnet can be regarded as the nonlinear restoring force $F_r$, that is

$$F_r = Ky\left(t\right) + F_m \tag{2}$$

Since the potential well plays a significant role in performance enhancement of multi-stable energy harvesters, it is necessary to investigate the potential well of multi-stable energy harvesters. The potential well can be calculated by the integrating nonlinear restoring force $F_r$ with respect to the displacement.

It has been widely acknowledged that the piezoelectric cantilever energy harvester without any magnets is regarded as a linear system. Therefore, the $K$ can be considered as a constant. Besides, in some magnetic configurations, the beam may have a large static deflection, so that the linear elastic force should be replaced by the nonlinear elastic force with the geometric nonlinearities.

Although the relationship between the nonlinear restoring force and dynamic performance of multi-stable energy harvesters has been verified experimentally (Cao et al., 2015), the mechanism by which the structural parameters influence the nonlinear restoring force must be understood. Once the relationship between structural parameters and nonlinear restoring force is understood, it aids in the design of the preferable nonlinear restoring force for performance enhancement. During the modeling of nonlinear restoring force, it is difficult to calculate the magnetic force since the magnetic force is highly sensitive to the spatial position of the magnets. Therefore, it is essential to investigate the accuracy and the applicability of these modeling methods for magnetic force calculation. In addition, from Eq. (2), only the magnetic force along excitation direction is required to calculate the nonlinear restoring force.

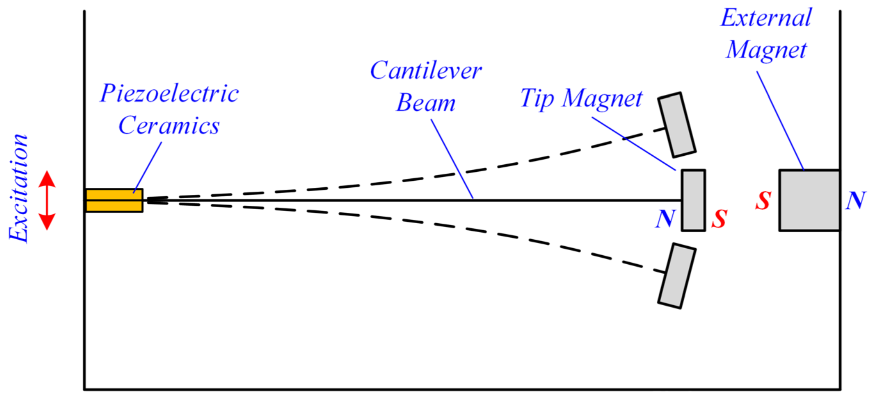


**Figure 1.** Schematic of bi-stable piezoelectric energy harvester

## 2.1 Modeling of magnetic force

The methods of modeling the magnetic force in multi-stable energy harvesters include magnetic dipole, improved dipole, magnetic current and magnetic charge methods. These methods can be applied to calculate the magnetic force between two permanent magnets. If there are more than one external magnets, the total magnetic force exerted on tip magnet can be obtained by superposing these magnetic forces. Taking the BPEH shown in Fig. 2 as an example, the magnetizations of the tip magnet and external magnet are denoted as $\mathbf{M}_1$ and $\mathbf{M}_2$ respectively, and the dimensions of the tip magnet and external magnet are $2a\times2b\times2c$ and $2A\times2B\times2C$ along $x$, $y$ and $z$ directions respectively. Before developing the model, the relationship between the rotational angle $\beta$ and the displacement $y$ of cantilever beam is required to define the spatial position of tip magnet. Based on the existing research (Friswell et al., 2012), the length of cantilever beam along $z$-direction versus displacement $y$ is

$$l_z = \frac{12l^3}{\pi^2 y^2 + 12l^2} \tag{3}$$

where $l$ is the original length of cantilever beam.

The rotational angle $\beta$ of cantilever beam at the free end is

$$\beta = \arcsin\left(\frac{\pi y}{2l\left(1-\cos\frac{\pi l_z}{2l}\right)}\sin\left(\frac{\pi l_z}{2l}\right)\right) \tag{4}$$

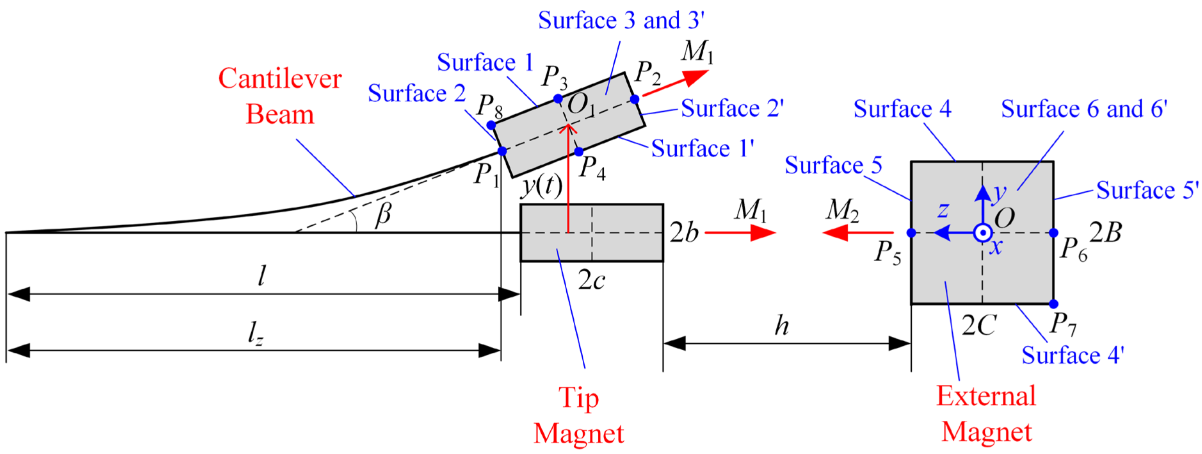


**Figure 2.** Modeling approach for a BPEH

### 2.2.1 Magnetic dipole method

The magnetic dipole method views the permanent magnet as a magnetic dipole point with an equivalent dipole moment to calculate magnetic field and magnetic force. As shown in Fig. 2, the equivalent magnetic moments of the tip magnet and external magnet in BPEH are $\mathbf{m}_t$ and $\mathbf{m}_e$

respectively, which are located in the geometric center $O_1$ and $O$ of tip magnet and external magnet. The magnetic moment is defined as the product of the magnetization and the volume of the permanent magnet. Therefore, when the displacement of cantilever beam is $y$, the magnetic moments of the tip magnet and external magnet are

$$\mathbf{m}_t = \begin{pmatrix} 0 & 8abcM_1 \sin\beta & -8abcM_1 \cos\beta \end{pmatrix} \tag{5}$$

$$\mathbf{m}_e = \begin{pmatrix} 0 & 0 & 8ABCM_2 \end{pmatrix} \tag{6}$$

According to the magnetic Coulomb's law, the magnetic flux density at point $O_1$ produced by external magnet is

$$\mathbf{B}_{e,t} = -\frac{\mu_0}{4\pi} \nabla \frac{\mathbf{m}_e \cdot \mathbf{r}_{OO_1}}{\left|\mathbf{r}_{OO_1}\right|^3} \tag{7}$$

where $\mu_0$ is the permeability in vacuum; $\mathbf{r}_{OO_1}$ represents the distance vector from the center of external magnet to the center of tip magnet, which can be expressed as

$$\mathbf{r}_{OO_1} = \begin{pmatrix} 0 & \omega & h + C + 2c + l - l_z - c\cos\beta \end{pmatrix} \tag{8}$$

Hence, the magnetic force on tip magnet exerted by the external magnet is

$$\mathbf{F}_{dipole} = -\nabla\left(-\mathbf{B}_{e,t} \cdot \mathbf{m}_t\right) = -\frac{\mu_0}{4\pi} \nabla\left(\left(\nabla \frac{\mathbf{m}_e \cdot \mathbf{r}_{OO_1}}{\left|\mathbf{r}_{OO_1}\right|^3}\right) \cdot \mathbf{m}_t\right) \tag{9}$$

After further calculation, Eq. (9) can be simplified as (Yung et al., 1998)

$$\mathbf{F}_{dipole} = \frac{3\mu_0}{4\pi\left|\mathbf{r}_{OO_1}\right|^5}\left(\mathbf{r}_{OO_1}\left(\mathbf{m}_t \cdot \mathbf{m}_e\right) + \mathbf{m}_t\left(\mathbf{r}_{OO_1} \cdot \mathbf{m}_e\right) + \mathbf{m}_e\left(\mathbf{r}_{OO_1} \cdot \mathbf{m}_t\right) - 5\mathbf{r}_{OO_1}\left(\frac{\mathbf{r}_{OO_1}}{\left|\mathbf{r}_{OO_1}\right|} \cdot \mathbf{m}_t\right)\left(\frac{\mathbf{r}_{OO_1}}{\left|\mathbf{r}_{OO_1}\right|} \cdot \mathbf{m}_e\right)\right) \tag{10}$$

Since only the volume and the magnetization of the magnet are considered when calculating the magnetic moment, this may yield an error in magnetic force calculation. If the magnetization and the volume of magnets are the same, the calculated magnetic moments are equal to each other since the shape of the magnets is ignored. It can be directly concluded that when the size of magnets is small and the separation between magnets is large, the magnets can be regarded as dipole points to improve the accuracy of magnetic dipole method.

### 2.2.2 Improved dipole method

The improved dipole method considers the magnetization of the permanent magnet as magnetic dipole points distributed on two magnetic surfaces, which are perpendicular to the direction of magnetization. Compared with magnetic dipole method, the dipoles of the improved dipole method are located in the center of two magnetic surfaces and there exist two dipoles for one magnet. Here, the magnetic surfaces of tip magnet and external magnet are surfaces 2, 2' and surfaces 5, 5' respectively in Fig. 2. The magnetic force between the tip magnet and the external magnet can be calculated by the magnetic Coulomb's law. As the displacement of cantilever beam is $y$, the centers of magnetic surfaces for tip magnet are $P_1\,(0, y - c\sin\beta, h+C+2c+l-l_z)$ and $P_2\,(0, y + c\sin\beta, h+C+2c+l-l_z-2c\cos\beta)$ respectively, while the centers of magnetic surfaces for external magnet are $P_5\,(0, 0, C)$ and $P_6\,(0, 0, -C)$ respectively. The surface magnetic dipole moments of $P_1$, $P_2$, $P_5$ and $P_6$ are defined as (Wang et al., 2019)

$$\begin{aligned} Q_1 &= -M_1 S_1 \\ Q_2 &= M_1 S_2 \\ Q_5 &= M_2 S_5 \\ Q_6 &= -M_2 S_6 \end{aligned} \tag{11}$$

where $S_1$, $S_2$, $S_5$, $S_6$ are the areas of magnetic surfaces at $P_1$, $P_2$, $P_5$, $P_6$, with $4ab$, $4ab$, $4AB$ and $4AB$ respectively.

The distance vectors from $P_1$ to $P_5$, $P_1$ to $P_6$, $P_2$ to $P_5$, $P_2$ to $P_6$ are

$$\begin{aligned} \mathbf{r}_{15} &= \mathbf{P}_1 - \mathbf{P}_5 \\ \mathbf{r}_{16} &= \mathbf{P}_1 - \mathbf{P}_6 \\ \mathbf{r}_{25} &= \mathbf{P}_2 - \mathbf{P}_5 \\ \mathbf{r}_{26} &= \mathbf{P}_2 - \mathbf{P}_6 \end{aligned} \tag{12}$$

Then, the magnetic flux density of point $P_1$ generated by external magnet is

$$\mathbf{B}_{P1} = \frac{\mu_0}{4\pi}\left( Q_5 \frac{\mathbf{r}_{15}}{\left|\mathbf{r}_{15}\right|^3} + Q_6 \frac{\mathbf{r}_{16}}{\left|\mathbf{r}_{16}\right|^3} \right) \tag{13}$$

The magnetic force of point $P_1$ is

$$\mathbf{F}_{imp,1} = Q_1 \mathbf{B}_{P1} \tag{14}$$

Similarly, the magnetic flux density of point $P_2$ generated by external magnet is

$$\mathbf{B}_{P2} = \frac{\mu_0}{4\pi}\left( Q_5 \frac{\mathbf{r}_{25}}{\left|\mathbf{r}_{25}\right|^3} + Q_6 \frac{\mathbf{r}_{26}}{\left|\mathbf{r}_{26}\right|^3} \right) \tag{15}$$

The magnetic force of point $P_2$ is

$$\mathbf{F}_{imp,2} = Q_2 \mathbf{B}_{P2} \tag{16}$$

As a result, the total magnetic force acted on tip magnet is

$$\mathbf{F}_{imp} = \mathbf{F}_{imp,1} + \mathbf{F}_{imp,2} \tag{17}$$

Since the improved dipole method regards the magnetization of magnets as a dipole located on the magnetic surfaces, the distribution of the magnetic surfaces has been ignored in the magnetic force calculation. If the area of the magnetic surfaces is small or the length along the magnetization direction of magnet is large, the magnetic surfaces can be approximately regarded as points.

### 2.2.3 Magnetic current method

The magnetic current method regards the magnetization of permanent magnets as a magnetic surface current density $\mathbf{K}_m$ and magnetic volume current density $\mathbf{J}_m$. The magnet with a magnetization $\mathbf{M}$ can be defined as

$$\begin{aligned} \mathbf{J}_m &= \nabla \times \mathbf{M} \\ \mathbf{K}_m &= \mathbf{M} \times \mathbf{n} \end{aligned} \tag{18}$$

where **n** is the unit vector of magnetization direction.

For uniformly magnetized magnets, the magnetization **M** is a constant, so that the magnetic volume current density $\mathbf{J}_m = 0$ and the magnitude of magnetic surface current density $\mathbf{K}_m$ is equal to the magnitude of magnetization **M**. Therefore, based on the Biot–Savart's law and the Kelvin equation, the incremental magnetic force ($\mathrm{d}\boldsymbol{F}_{\mathrm{cur}}$) of the tip magnet generated by the external magnet on an infinitesimal element (d$s$) is

$$\mathrm{d}\mathbf{F}_{cur} = \mu_0 \nabla \left( \mathbf{M}_1 \cdot \mathbf{H}_{ext} \right) \mathrm{d}s \tag{19}$$

where $\mathbf{H}_{ext}$ is the magnetic field produced by external magnet.

According to Ampere's rule, the equivalent current density distributed at the tip magnet is described in Fig. 3. In this method, the rotational angle $\beta$ of the cantilever beam is assumed very small, so that only the current density distributed on surface 1 and surface 1' which are perpendicular to the $y$ direction can contribute to the magnetic force along the $y$ direction. To obtain a total magnetic force, there is a need to calculate and integrate the magnetic flux density produced on the whole surface 1 and 1'; however, it is difficult to calculate the magnetic flux density directly because of the complexity of distribution. Therefore, the current density distributed on surface 1 and 1' is simply equivalent to the current density at the surface centers $P_3$ $(0, y + b\cos\beta, h + C + 2c + l - l_z - c\cos\beta + b\sin\beta)$ and $P_4$ $(0, y - b\cos\beta, h + C + 2c + l - l_z - c\cos\beta - b\sin\beta)$. As a result, the magnetic flux density of surface center is only required to calculate the magnetic force (Gao et al., 2016). The magnetic force of tip magnet along $y$ direction is given by

$$\begin{aligned} \mathbf{F}_{cur,y} &= \iint_S M_1 \mu_0 \mathbf{H}_{z4}(s)\,\mathrm{d}s - \iint_S M_1 \mu_0 \mathbf{H}_{z3}(s)\,\mathrm{d}s \\ &= M_1 \mu_0 S \left( H_{z4}(P_4) - H_{z3}(P_3) \right) \end{aligned} \tag{20}$$

where $\mathbf{H}_{z3}(s)$ and $\mathbf{H}_{z4}(s)$ are the magnetic fields of surface 1 and surface 1' along $z$ direction produced by external magnet; $H_{z3}(P_3)$ and $H_{z4}(P_4)$ are the magnetic fields of $P_3$ and $P_4$ along $z$ direction produced by external magnet; $S$ is the area of both surface 1 and surface 1' and equals $4ac$.

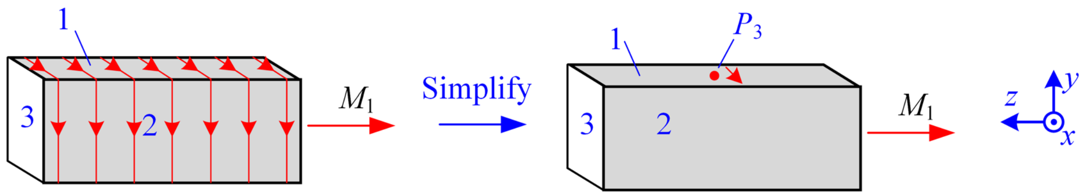


**Figure 3.** Equivalent magnetic current of tip magnet

Then, the magnetic field produced by the external magnet is calculated by the magnetic charge method. Here, it is assumed that the coordinates of points $P_3$ and $P_4$ are $(x_3, y_3, z_3)$ and $(x_4, y_4, z_4)$. Therefore, the magnetic fields along $z$ directions of $P_3$ and $P_4$ produced by external magnet are given by (Akoun and Yonnet, 1984)

$$\begin{aligned} H_{z3} = &\left(\frac{M_2}{4\pi}\right)\left(\arctan\left(\frac{(x_3+A)(y_3+B)}{z_3\sqrt{(x_3+A)^2+(y_3+B)^2+z_3^2}}\right)+\arctan\left(\frac{(x_3-A)(y_3-B)}{z_3\sqrt{(x_3-A)^2+(y_3-B)^2+z_3^2}}\right)\right) \\ &-\left(\frac{M_2}{4\pi}\right)\left(\arctan\left(\frac{(x_3-A)(y_3+B)}{z_3\sqrt{(x_3-A)^2+(y_3+B)^2+z_3^2}}\right)-\arctan\left(\frac{(x_3+A)(y_3-B)}{z_3\sqrt{(x_3+A)^2+(y_3-B)^2+z_3^2}}\right)\right) \end{aligned} \tag{21}$$

$$\begin{aligned} H_{z4} = &\left(\frac{M_2}{4\pi}\right)\left(\arctan\left(\frac{(x_4+A)(y_4+B)}{z_4\sqrt{(x_4+A)^2+(y_4+B)^2+z_4^2}}\right)+\arctan\left(\frac{(x_4-A)(y_4-B)}{z_4\sqrt{(x_4-A)^2+(y_4-B)^2+z_4^2}}\right)\right) \\ &-\left(\frac{M_2}{4\pi}\right)\left(\arctan\left(\frac{(x_4-A)(y_4+B)}{z_4\sqrt{(x_4-A)^2+(y_4+B)^2+z_4^2}}\right)-\arctan\left(\frac{(x_4+A)(y_4-B)}{z_4\sqrt{(x_4+A)^2+(y_4-B)^2+z_4^2}}\right)\right) \end{aligned} \tag{22}$$

### 2.2.4 Magnetic charge method

The magnetic charge method considers that the magnetization of the permanent magnet as positive and negative magnetic charges distributed on two magnetic surfaces. Then, according to Coulomb's magnetic law, the magnetic potential energy can be obtained to calculate the magnetic force. In particular, the magnetic charge of the tip magnet is distributed on surface 2 and 2', while the magnetic charge of the external magnet is distributed on surface 5 and 5'. The magnetic charge densities of surface 2, 2', 5 and 5' are

$$\begin{aligned} \sigma_2 &= \mu_0 \left|\mathbf{M}_1\right| \\ \sigma_{2'} &= -\mu_0 \left|\mathbf{M}_1\right| \\ \sigma_5 &= \mu_0 \left|\mathbf{M}_2\right| \\ \sigma_{5'} &= -\mu_0 \left|\mathbf{M}_2\right| \end{aligned} \tag{23}$$

Considering surface 2 and surface 5, the interaction energy is

$$W_{2,5} = \int_{-a}^{a} \mathrm{d}x \int_{-b}^{b} \mathrm{d}y \int_{-A}^{A} \mathrm{d}X \int_{-B}^{B} \mathrm{d}Y \frac{\sigma_2 \sigma_5}{4\pi\mu_0 r} \tag{24}$$

where $r$ is the distance between two magnetic charge densities on surface 2 and surface 5; $x$, $y$, $X$ and $Y$ are the dummy variables.

After integrations, the total interaction energy is

$$W = W_{2,5} + W_{2,5'} + W_{2',5} + W_{2',5'} \tag{25}$$

The magnetic force can be obtained by

$$\mathbf{F}_{cha} = \nabla W \tag{26}$$

First, when the rotational angle $\beta$ of cantilever beam is 0, the tip magnet and external magnet are parallel with each other. It is assumed that the differences between the two geometric centers of the tip magnet and external magnet along $x$, $y$, $z$ directions are $\alpha_1$, $\beta_1$ and $\gamma_1$ respectively. Then, the magnetic potential energy after integration is given by (Akoun and Yonnet, 1984)

$$W = \frac{\mu_0 M_1 M_2}{4\pi} \sum_{i=0}^{1} \sum_{j=0}^{1} \sum_{k=0}^{1} \sum_{l=0}^{1} \sum_{p=0}^{1} \sum_{q=0}^{1} (-1)^{i+j+k+l+p+q} \psi\left(u_{ij}, v_{kl}, w_{pq}, r\right) \tag{27}$$

where $i, j, k, l, p$ and $q$ are the dummy variables; $u$, $v$, $w$ and $r$ are the intermediate variables;

$$\psi\left(u_{ij}, v_{kl}, w_{pq}, r\right) = \frac{1}{2}u\left(v^2 - w^2\right)\ln\left(r-u\right) + \frac{1}{2}v\left(u^2 - w^2\right)\ln\left(r-v\right) + uvw\arctan\frac{uv}{rw} + \frac{r}{6}\left(u^2 + v^2 - 2w^2\right) \quad (28)$$

$$\begin{aligned} u_{ij} &= \alpha_1 + (-1)^j A - (-1)^i a \\ v_{kl} &= \beta_1 + (-1)^l B - (-1)^k b \\ w_{pq} &= \gamma_1 + (-1)^q C - (-1)^p c \\ r &= \sqrt{u_{ij}^2 + v_{kl}^2 + w_{pq}^2} \end{aligned} \quad (29)$$

After calculation of the gradient of magnetic potential energy, the magnetic force between the tip magnet and external magnet is

$$F_{cha} = \frac{\mu_0 M_1 M_2}{4\pi}\sum_{i=0}^{1}\sum_{j=0}^{1}\sum_{k=0}^{1}\sum_{l=0}^{1}\sum_{p=0}^{1}\sum_{q=0}^{1}(-1)^{i+j+k+l+p+q}\,\phi\left(u_{ij}, v_{kl}, w_{pq}, r\right) \quad (30)$$

where for magnetic force $F_{cha,y}$ along $y$ direction, it has

$$\phi = \frac{1}{2}\left(u^2 - w^2\right)\ln\left(r-v\right) + uv\ln\left(r-u\right) + uw\arctan\frac{uv}{rw} + \frac{1}{2}rv \quad (31)$$

Second, if the rotational angle $\beta$ of the cantilever beam is not equal to $k\pi$ ($k$ = 1,2,3…), the rotational angle of the magnetization direction for the tip magnet relative to the external magnet along the counter-clockwise direction is $\pi+\beta$. On selecting the vertexes of the external magnet and tip magnet $P_7$ ($-A$, $-B$, $-C$) and $P_8$ ($-a$, $(y/\sin\beta - c)\sin\beta + b\cos\beta$, $h + C + 2c + l + l_z + b\sin\beta$), the relative difference between $P_7$ and $P_8$ is

$$\begin{aligned} x_{01} &= -a + A \\ y_{01} &= \left(y/\sin\beta - c\right)\sin\beta + b\cos\beta + B \\ z_{01} &= h + C + 2c + l + l_z + b\sin\beta \end{aligned} \quad (32)$$

Therefore, the magnetic force along the $z$ direction is expressed from Eq. (33) to Eq. (39) where $f_1$, $f_2$, $f_3$, $f_4$, $f_5$, $f_6$ are intermediate functions and $u$, $v$, $w$, $y'$ and $z'$ are the intermediate variables (Charpentier and Lemarquand, 1999).

$$
\begin{aligned}
F_y\left(\pi+\beta, x_{01}, y_{01}, z_{01}, A, B, C, a, b, c, M_1, M_2\right) = & f_1\left(x_{01}, x_{01}+a, y_{01}, z_{01}, \pi+\beta, 0, 0, b, c, M_1, M_2\right) \\
& -f_1\left(x_{01}-A, x_{01}-A+a, y_{01}, z_{01}, \pi+\beta, 0, 0, b, c, M_1, M_2\right) \\
& +f_1\left(x_{01}-A, x_{01}-A+a, y_{01}, z_{01}, \pi+\beta, B, 0, b, c, M_1, M_2\right) \\
& -f_1\left(x_{01}, x_{01}+a, y_{01}, z_{01}, \pi+\beta, B, 0, b, c, M_1, M_2\right) \\
& +f_1\left(x_{01}-A, x_{01}-A+a, y_{01}, z_{01}, \pi+\beta, 0, C, b, c, M_1, M_2\right) \\
& -f_1\left(x_{01}, x_{01}+a, y_{01}, z_{01}, \pi+\beta, 0, C, b, c, M_1, M_2\right) \\
& +f_1\left(x_{01}, x_{01}+a, y_{01}, z_{01}, \pi+\beta, B, C, b, c, M_1, M_2\right) \\
& -f_1\left(x_{01}-A, x_{01}-A+a, y_{01}, z_{01}, \pi+\beta, B, C, b, c, M_1, M_2\right)
\end{aligned} \tag{33}
$$

$$
\begin{aligned}
f_1\left(v, w, y_{01}, z_{01}, \pi+\beta, B, C, b, c, M_1, M_2\right) = & \frac{M_1 M_2}{4\pi\mu_0}\left(f_2\left(v, w, y_{01}, z_{01}, \pi+\beta, B, C, b, c\right)\right. \\
& \left.-f_2\left(v, w, y_{01}, z_{01}, \pi+\beta, B, C, b, 0\right)\right)
\end{aligned} \tag{34}
$$

$$
\begin{aligned}
f_2\left(v, w, y_{01}, z_{01}, \pi+\beta, B, C, b, z'\right) = & f_3\left(w, y_{01}, z_{01}, \pi+\beta, B, C, 0, z'\right) - f_3\left(v, y_{01}, z_{01}, \pi+\beta, B, C, b, z'\right) \\
& -f_3\left(w, y_{01}, z_{01}, \pi+\beta, B, C, 0, z'\right) + f_3\left(v, y_{01}, z_{01}, \pi+\beta, B, C, 0, z'\right)
\end{aligned} \tag{35}
$$

$$
\begin{aligned}
f_3\left(u, y_{01}, z_{01}, \pi+\beta, B, C, y', z'\right) = & u f_6\left(y_{01}, z_{01}, \pi+\beta, B, C, y'\right) \ln\left(-u + f_4\left(y_{01}, z_{01}, \pi+\beta, B, C, y', z'\right)\right) \\
& -u f_6\left(y_{01}, z_{01}, \pi+\beta, B, C, y'\right) \\
& -u^2 \ln\left(f_4\left(y_{01}, z_{01}, \pi+\beta, B, C, y', z'\right) + f_6\left(y_{01}, z_{01}, \pi+\beta, B, C, y'\right)\right) \\
& +u f_5\left(y_{01}, z_{01}, \pi+\beta, B, C, z'\right) \arctan\left(\frac{-f_5^2\left(y_{01}, z_{01}, \pi+\beta, B, C, y'\right) - u^2 + u f_4\left(y_{01}, z_{01}, \pi+\beta, B, C, y', z'\right)}{f_5\left(y_{01}, z_{01}, \pi+\beta, B, C, z'\right) f_6\left(y_{01}, z_{01}, \pi+\beta, B, C, y'\right)}\right) \\
& +\frac{1}{2} u\pi \left|f_5\left(y_{01}, z_{01}, \pi+\beta, B, C, z'\right)\right| sign\left(f_6\left(y_{01}, z_{01}, \pi+\beta, B, C, y'\right)\right) \\
& +\frac{1}{2} f_6\left(y_{01}, z_{01}, \pi+\beta, B, C, y'\right) f_4\left(y_{01}, z_{01}, \pi+\beta, B, C, y', z'\right) \\
& +\frac{1}{2}\left(u^2 + f_5^2\left(y_{01}, z_{01}, \pi+\beta, B, C, y', z'\right)\right) \ln\left(f_4\left(y_{01}, z_{01}, \pi+\beta, B, C, y', z'\right) + f_6\left(y_{01}, z_{01}, \pi+\beta, B, C, y'\right)\right)
\end{aligned} \tag{36}
$$

$$
f_4\left(y_{01}, z_{01}, \pi+\beta, B, C, y', z'\right) = \sqrt{u^2 + f_5^2\left(y_{01}, z_{01}, \pi+\beta, B, C, z'\right) + f_6^2\left(y_{01}, z_{01}, \pi+\beta, B, C, y'\right)} \tag{37}
$$

$$
f_5\left(y_{01}, z_{01}, \pi+\beta, B, C, z'\right) = -y_{01}\sin\left(\pi+\beta\right) + z_{01}\cos\left(\pi+\beta\right) + b\sin\left(\pi+\beta\right) - c\cos\left(\pi+\beta\right) + z' \tag{38}
$$

$$
f_6\left(y_{01}, z_{01}, \pi+\beta, B, C, y'\right) = y_{01}\cos\left(\pi+\beta\right) + z_{01}\sin\left(\pi+\beta\right) - B\cos\left(\pi+\beta\right) - C\sin\left(\pi+\beta\right) + y' \tag{39}
$$

Therefore, the magnetic force calculated by the magnetic charge method is via integrating the magnetic force between surfaces to obtain the theoretical expression.

## 3 Numerical simulations for applicability analysis

Numerical simulation is applied here to investigate the application constraints of these four different modeling methods for calculation of the magnetic force. Several structural parameters and magnets sizes are taken into consideration, including the ratio $\zeta$ of the magnetic surface area to the length along the magnetization direction, the distance $h$ between magnets, the length along $x$, $y$ and $z$ directions. In this part, the mechanisms by which these factors influence the accuracy of the calculation of magnetic force is analyzed, and the quantitative errors of different methods are determined and compared. According to this result, the application constraints and applicability of these modeling methods could be concluded.

The process of simulation is achieved by AC/DC modules of COMSOL. The original length of cantilever beam is 120 mm, and the magnet is N50 with a magnetization of 1.41 T. In addition, the theoretical magnetic forces of magnetic dipole, improved dipole, magnetic current and magnetic charge methods are from the above analytical expressions.

**3.1 Ratio of magnetic surface area to length along magnetization direction**

The ratio of the magnetic surface area to the length along the magnetization direction is defined as $\zeta = 4AB/2C = 4ab/2c$, as shown in Fig. 2, and the dimensions of the tip magnet and the external magnet are the same. The terms $2A$ and $2B$ are the lengths along the $x$ and $y$ directions, thereby constructing the magnetic surface of the tip magnet. The dimension $2C$ is the length along the $z$ direction, namely the magnetization direction. Figure 4 indicates the influence of $\zeta$ on the magnetic force, where $h$ is 10 mm. It can be seen that with a decrease of $\zeta$, the magnetic force from the improved dipole method is in better agreement with the numerical result. This may be because the magnetic surfaces can be regarded as points when the area of the magnetic surfaces is much smaller than the length along the magnetization direction. When $\zeta = 0.4$, the error in the peak value between the improved dipole method and the numerical result is 9.25%, but this error increases dramatically when $\zeta$ reaches 2.5. In addition, the magnetic charge method matches well with the numerical result under different values of ζ, and the errors exhibit a lower difference, which stabilizes at around 3%. In addition, during an increase of ζ from 0.4 to 2.5, the errors for the magnetic dipole method and magnetic current method both exhibit a small decline, but show a large deviation. This may be due the fact that for large ζ, magnets can no longer be regarded as dipoles, and the influence of the magnet shape significantly decreases the accuracy of magnetic dipole method.

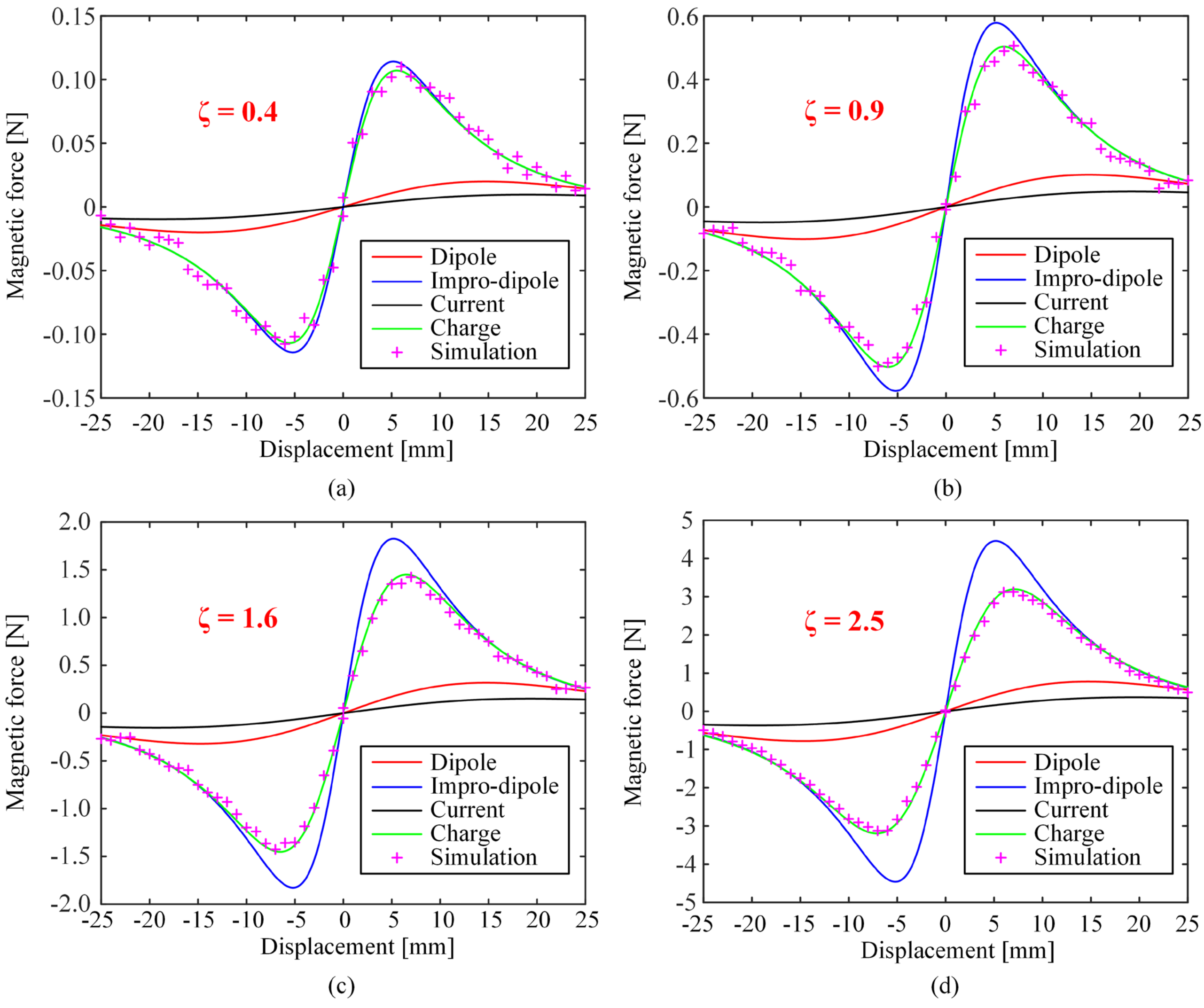


**Figure 4.** Influence of the ratio ζ of magnetic surface area to the length along magnetization

### 3.2 Distance between magnets

The parameter $h$ is considered here, as shown in Fig. 2, to analyze the influence of the structural parameters. Figure 5 shows the influence of $h$ on the magnetic force, and the other parameters in this system are $2A = 2a = 10$ mm, $2B = 2b = 10$ mm, $2C = 2c = 10$ mm. The results indicate that when $h$ increases from 5 mm to 20 mm, the magnetic forces obtained by magnetic dipole method and improved dipole method become more consistent with the numerical results. This may be due to the fact that if the tip magnet and external magnet are far from each other, the dipoles in these two methods can approximately represent the magnets. In detail, with an increase in $h$ from 5 mm to 20 mm, the errors of the peak values of the improved dipole method and magnetic dipole method decrease to 25.5% and to 15.2% respectively. In addition, compared with the numerical result, the magnetic force calculated by the magnetic current method is increasingly higher during the increase in $h$. When $h$ is 5 mm, the magnetic force predicted by the magnetic current method is lower than the numerical simulation, with an error of 18.0%. When $h$ increases to 10 mm, the magnetic forces between the magnetic current method and numerical result are in good agreement, with an error of only 6.5%. However, with a continuous rise of $h$ from 15 mm to 20 mm, the error in a magnetic current has a significant rise. As for magnetic charge method, the errors show lower difference, with a figure of around 5%.

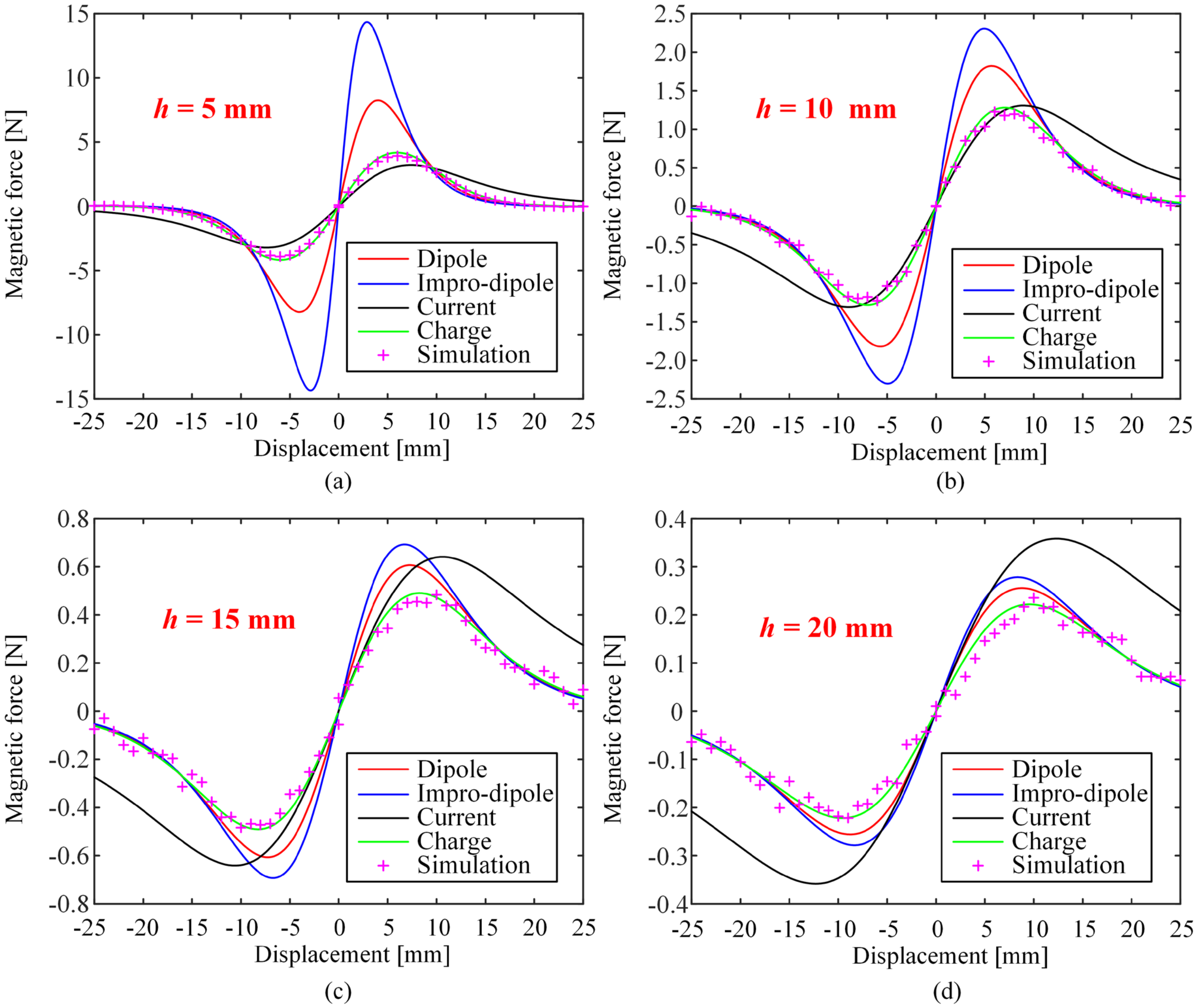


**Figure 5.** Influence of the distance *h* between magnets

### 3.3 Length along *x* direction

The length of magnet along the *x* direction is now considered to investigate the influence on magnetic force calculation as shown in Fig. 6. In this figure, $2A$ and $2a$ are the lengths of the external magnet and tip magnet along the *x* direction respectively, the other parameters are $2B = 2b = 10$ mm, $2C = 2c = 10$ mm and $h = 10$ mm. The improved dipole method shows a large difference compared with the numerical result and the error increases when the length of the magnet along the *x* direction increases from 6 mm to 18 mm. This may be caused by the increase in the length along the *x* direction, which increases the area of the magnetic surface, thus the magnetic surface can no longer be regarded as a dipole. In addition, the magnetic current method also sees a large deviation, but the error falls to 25.2%. For the magnetic dipole method, the error first decreases but then increases with the increase of the length of magnet along the *x* direction. In detail, when the lengths along the *x* direction are 6 mm and 10 mm, the errors are 7.9% and 6.5 % respectively. When the length along the *x* direction increases to 18 mm, the error can be 37.1%. Besides, the errors in magnetic force between the magnetic charge method and numerical result are stabilized at around 5% during the whole process.

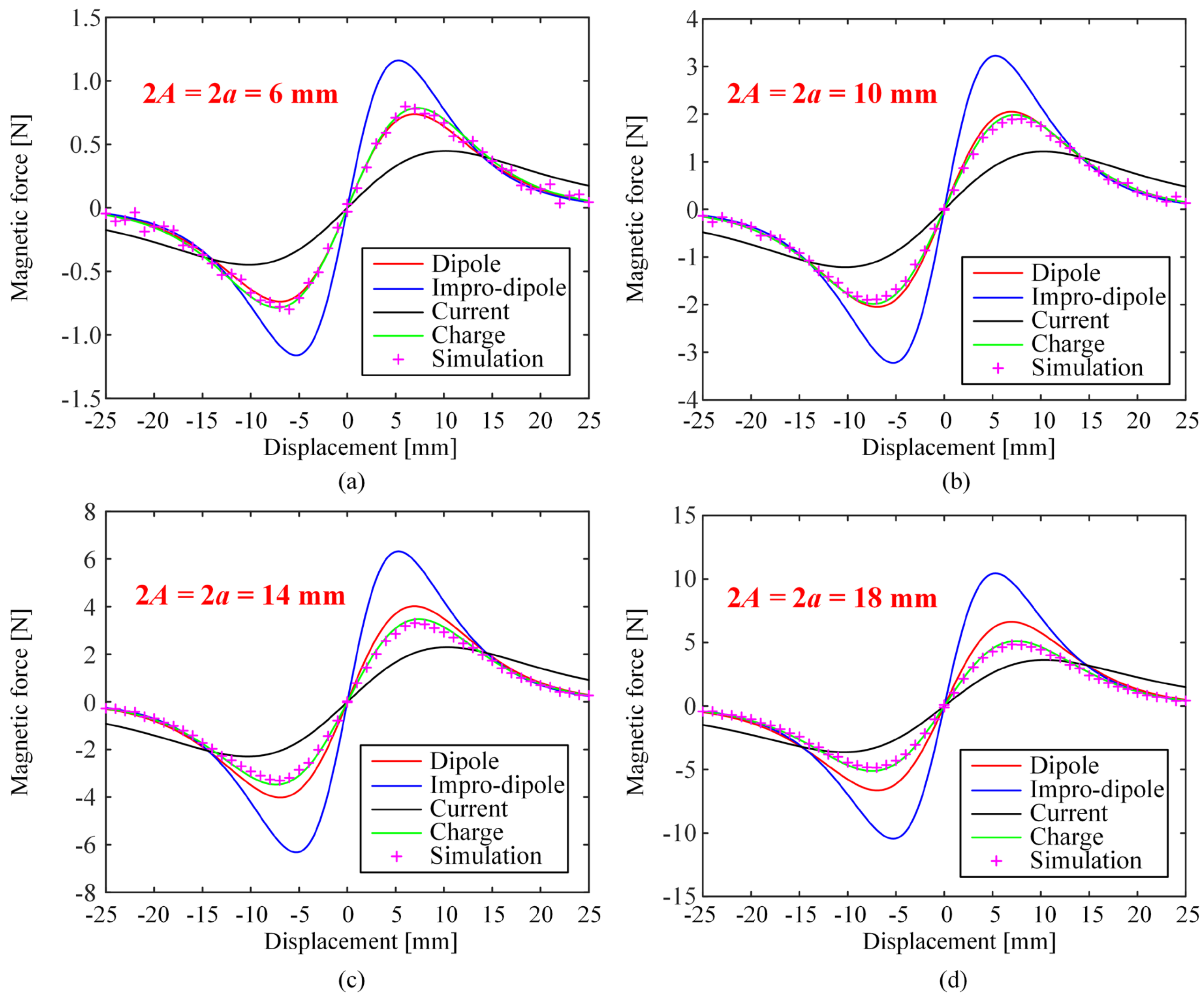


**Figure 6.** Influence of the length along *x* direction

### 3.4 Length along *y* direction

Figure 7 analyzes the influence of the length along the $y$ direction on the magnetic force. In this figure, $2B$ and $2b$ are the lengths of the external magnet and tip magnet along the $y$ direction respectively, the other parameters are $2A = 2a = 8$ mm, $2C = 2c = 8$ mm and $h = 10$ mm. It can be seen that with an increase of the length along the $y$ direction from 4 mm to 16 mm, the magnetic force predicted by the magnetic current method approaches the simulation, with the error decreasing to 4.2%. This may be due to the increase of the length along the $y$ direction, where the area of the current surface has less influence on the distribution of the magnetic field, and therefore the current surface is likely to match the assumption of the magnetic current method. In addition, the error of the improved dipole method shows a significant increase trend with an increase of the length along the $y$ direction from 4 mm to 16 mm. For the magnetic dipole method, the error in the magnetic force first exhibits a decreasing trend and then an increasing trend with an increase of the length along the $y$ direction. In detail, it decreases from 13.5% to 2.1% when the length along the $y$ direction increases from 4 mm to 8 mm. For larger lengths, this error tends to climb to 74.6% when the length along $y$ direction is 16 mm. In addition, the magnetic charge method shows a small error of approximately 3%.

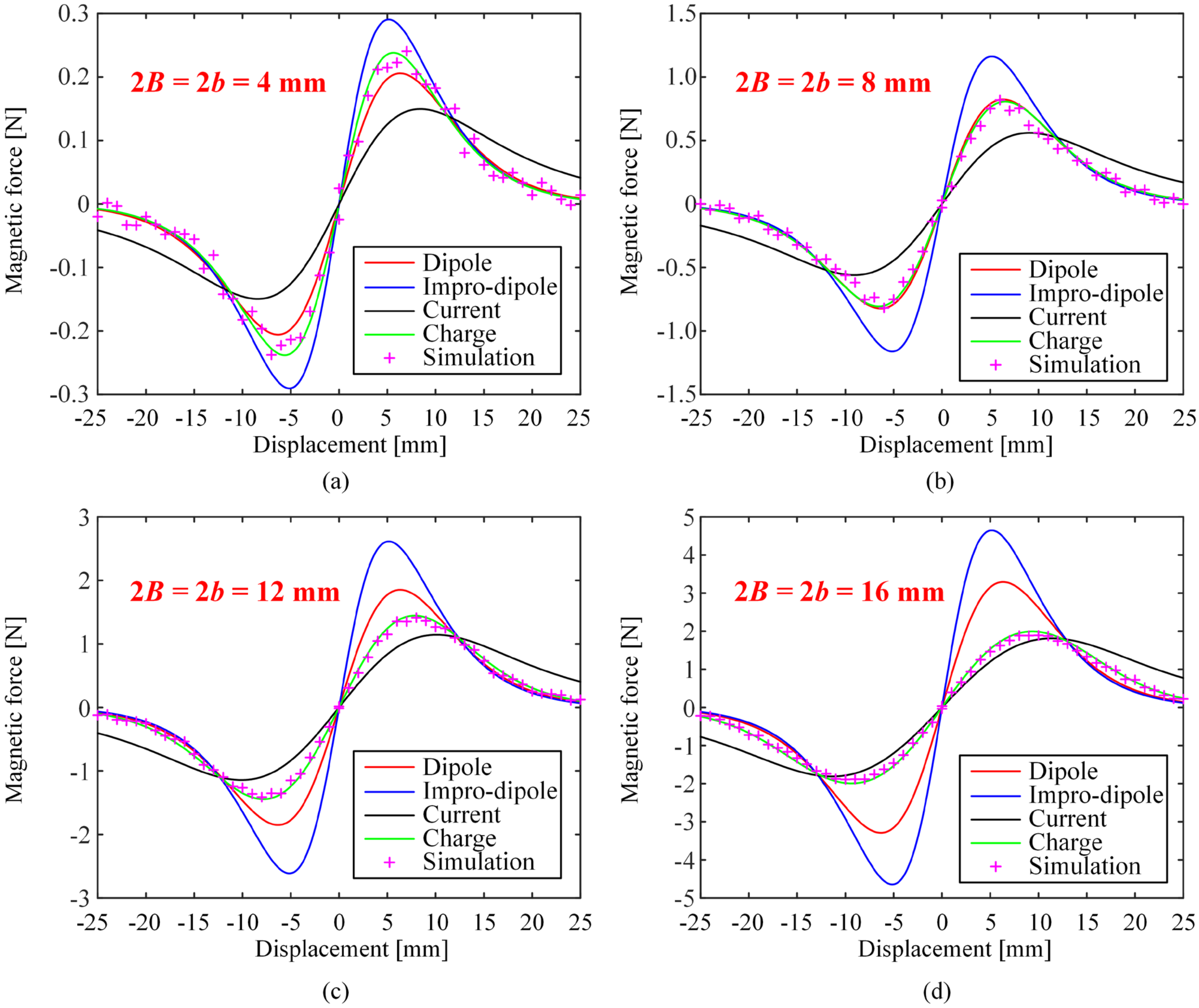


**Figure 7.** Influence of the length along *y* direction

### 3.5 Length along *z* direction

Figure 8 investigates the influence of the length along the *z* direction, where 2*C* and 2*c* are the lengths of external magnet and tip magnet along *z* direction respectively, the other parameters are 2*A* = 2*a* = 10 mm, 2*B* = 2*b* = 10 mm and *h* = 10 mm. This indicates that the magnetic force calculated by improved dipole method is closer to numerical result with an increase of the length along the *z* direction. In addition, during the increase in length along the *z* direction, the errors for the magnetic current method and magnetic dipole method both have a decreasing trend, but then show an increasing trend for longer lengths. When the length along the $z$ direction increases from 4 mm to 8 mm, the error of magnetic current method decreases to 6.4%, after which this error increase to 54.5%. Similarly, the error for the magnetic dipole method has a significant fall to 6.5%, with the length along the $z$ direction ranging from 4 mm to 10 mm. When the length along the $z$ direction increases to 14 mm, this error can increase to 15.8%. In addition, the errors for the magnetic charge method are about 5%.

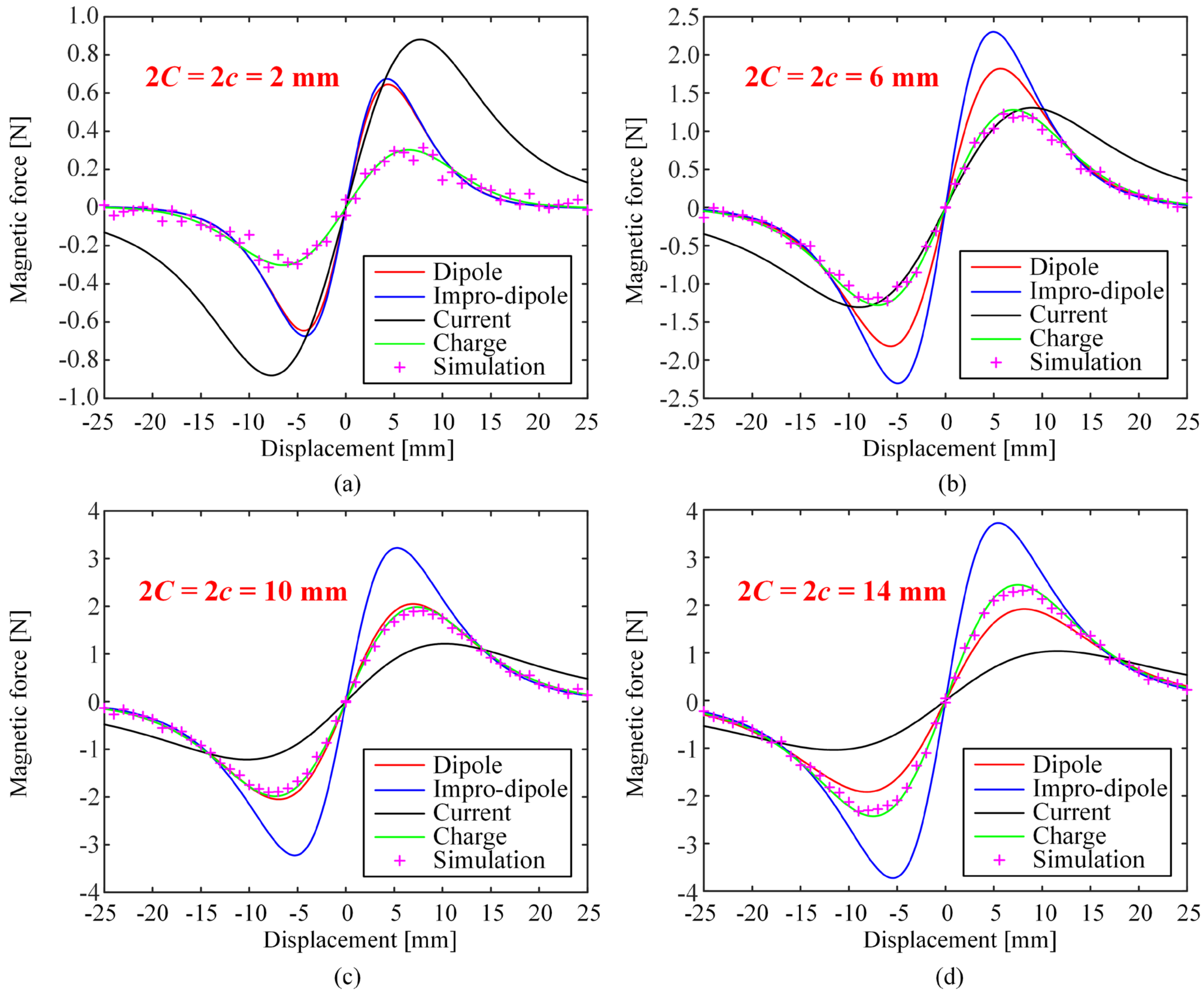


**Figure 8.** Influence of the length along $z$ direction

Therefore, the applicability of the above methods can now be concluded. Firstly, the improved dipole method is suitable for conditions where $\zeta$ is low in Fig. 4(a). This may be because in this condition the area of the magnetic surface is much lower than the length along the magnetization direction; as a result, the magnetic surface can be regarded as a dipole point, which satisfies the assumption of this method. However, when the lengths along $x$ and $y$ directions are high, as in Fig. 6(d) and Fig. 7(d), the area of the magnetic surface is increased and can no longer be ignored, thereby increasing the error for the improved dipole method.

Secondly, in the case of a large $h$, the improved dipole method and magnetic dipole method can both exhibit a high accuracy in Fig. 5(d). This may be caused by the assumption of a dipole point. For the improved dipole method and magnetic dipole method, the conditions of a large distance could match the assumption of dipole point.

Thirdly, the magnetic dipole method is preferable when all dimensions of magnets are equal to each other, as shown in Fig. 6 (b) and Fig. 7 (b), where the lengths along the $x$, $y$ and $z$ directions are all 10 mm and 8 mm respectively. In addition, smaller lengths can lead to higher accuracy for the magnetic dipole method. This phenomenon relies on the calculation of magnetic moment, only considering the volume and the magnetization of magnets. If all lengths of the magnets are the same, the magnetic moment could be approximately located in the geometric center of magnets.

In addition, the magnetic current method can be favorable if the length along the $y$ direction is relatively large. This may be because the area of the current surface is the product of the lengths along $x$ direction and $z$ direction. If the area of current surface is much smaller than the length along $y$ direction, the magnetic distribution on the current surface may be ignored to match the assumption of magnetic current method.

Finally, the magnetic charge method is able to have a relatively high accuracy for all occasions, with a maximal error of 5%, but this method could have more complicated expressions.

Moreover, some of the application constraints presented in this paper can match the finds in other literatures. It has reported that the larger error can be seen in dipole model compared to the improved dipole method in smaller gaps (Wang et al., 2019). It can be used to support the findings in this paper. In addition to the application of smaller gaps, the more comprehensive applicability of magnetic force models has been presented in this paper. The influence of structural parameters on the accuracy of magnetic force calculation has been deeply analyzed to obtain the application constraints of modeling methods under a range of operating conditions. These findings of application constraints will be helpful to provide a clear guideline for the application of magnetic force modeling methods.

## 4 Experimental verifications

In order to compare the relative accuracy of these methods, an experimental configuration has been developed to measure the magnetic force, as shown in Fig. 9. This configuration contains a dynamometer, laser displacement sensor, screw and multi-stable piezoelectric energy harvester. The dynamometer (Force Gauge Model M5-2) with a resolution of 0.002 N connects with an external magnet. A laser displacement sensor (Panasonic HL-G105-A -C5) with a resolution of 1.5 μm is used to obtain the displacement of the cantilever beam. The dimensions of the stainless steel cantilever beam are 120 mm × 10 mm × 0.28 mm, with a Young modulus of 200 GPa. The material of the tip magnet and external magnet is N50 with the magnetization of 1.46 T. The dimensions of the tip magnet and external magnet are 10 mm × 10 mm × 4 mm and 10 mm × 10 mm × 10 mm respectively. By adjusting the screw, the magnetic force and the displacement are recorded to obtain the magnetic force under different positions.

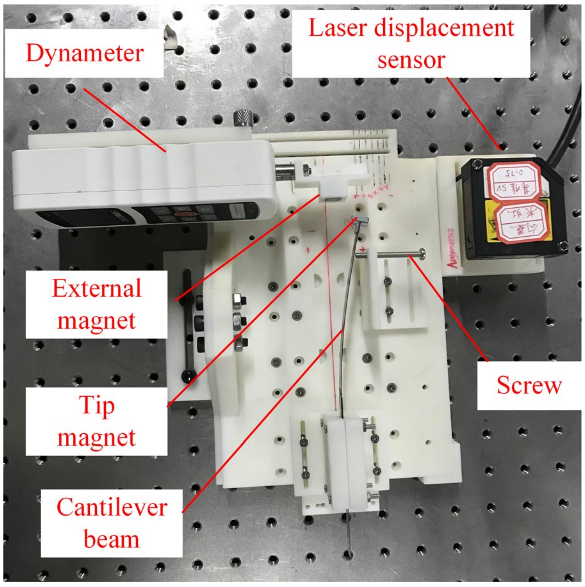


**Figure 9.** Experimental configuration for magnetic force measurement

### 4.1 Bi-stable piezoelectric energy harvester

Figure 10 shows the magnetic force of BPEH-1 and BPEH-2 for different $h$ of 12 mm and 22 mm. Here, the error of the peak value for the magnetic force is selected to investigate the accuracy of different modeling methods. During the increasing in $h$ from 12 mm to 22 mm, both magnetic forces of experimental measurement for BPEH-1 and BPEH-2 are in good agreement with the magnetic charge method, with the errors of 2.6% and 4.2% respectively. In addition, although the improved dipole method has more deviation from experimental result, the accuracy of improved dipole method can be significantly improved, with the error reducing from 61.5% to 26.0%. Similarly, the accuracy of the magnetic current method also sees a dramatic rise, with the error from 31.8% to 8.1%. The magnetic force calculated by magnetic current method is lower than the experimental result with $h$ of 12 mm, but it is higher than the experimental result when $h$ reaches 12 mm. In addition, the accuracy of the magnetic dipole method has a slight increase with a rise of $h$, with the error from 23% to 12.6%.

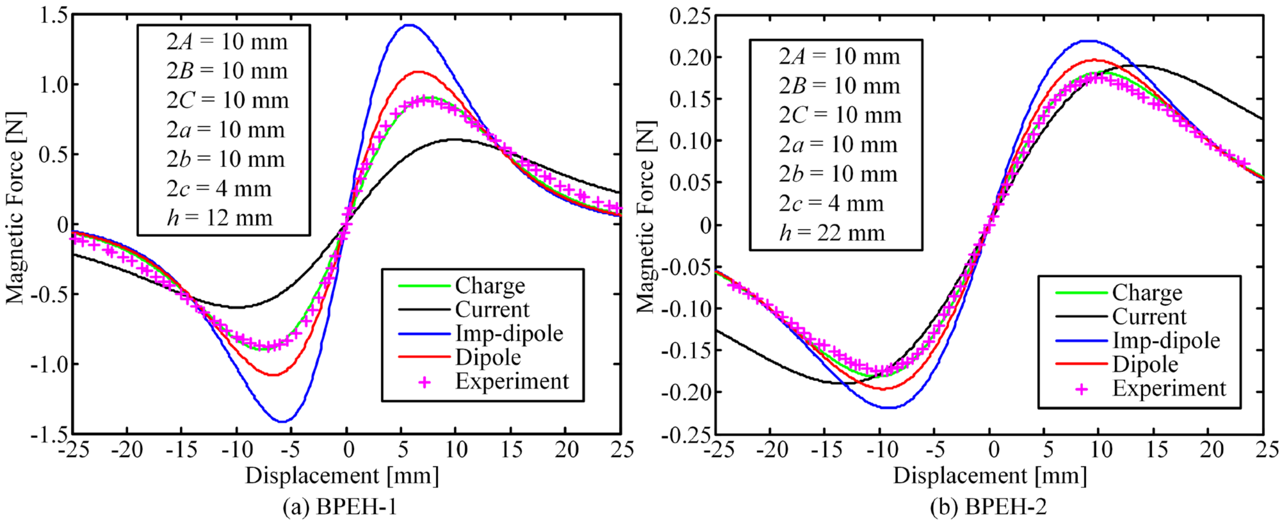


**Figure 10.** Experimental comparison for magnetic force of BPEH

### 4.2 Tri-stable piezoelectric energy harvester

The schematic of tri-stable piezoelectric energy harvester considered in the experimental test is shown in Fig.11. There are two external magnets compared with bi-stable piezoelectric energy harvester. The $d$ represents the distance between the two external magnets.

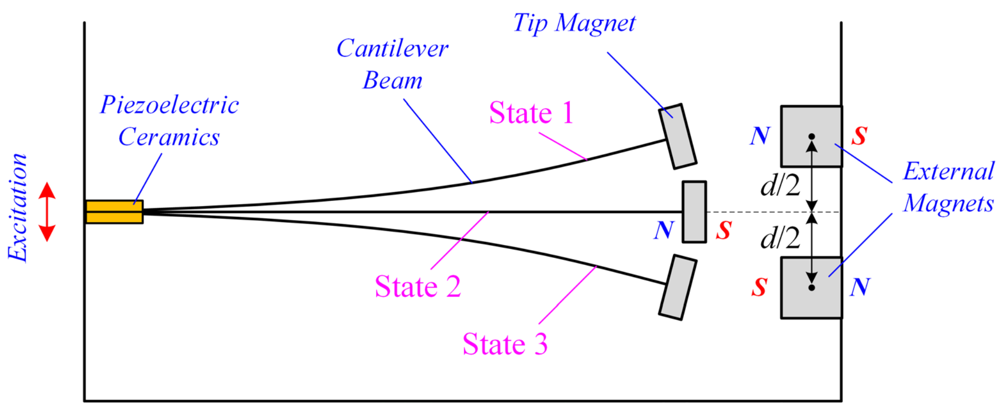


**Figure 11.** Schematic of tri-stable piezoelectric energy harvester

Figure 12 describes the magnetic forces of TPEH-1 and TPEH-2 for different $h$ of 12 mm and 14 mm, with the $d$ of 10 mm. Compared with the BPEH, the magnetic force of TPEH has two peak values which are defined as the *inner* peak value and the *outer* peak value. It can be observed that both magnetic forces of experimental measurement for TPEH-1 and TPEH-2 are consistent with magnetic charge method. The errors of the inner peak value and the outer peak value of magnetic charge method in TPEH-1 and TPEH-2 are 3.64% and 8.35%, 4.84% and 6.35% respectively. In terms of improved dipole method, during an increase of $h$, the errors of the inner peak value and the outer peak value have a decreasing trend, from 81.0% to 63.2% and from 56.2% to 45.6%. Similarly, the errors of the inner peak value and the outer peak value for magnetic dipole method also exhibit a slight decrease, from 33.6% to 24.4% and from 21.9% to 20.4% respectively. In contrast, the accuracy of the magnetic current method is reduced with an increase of $h$, with the error of the inner peak value from 83.3% to 90.3% and the error of outer peak value from 8.5% to 22.0%.

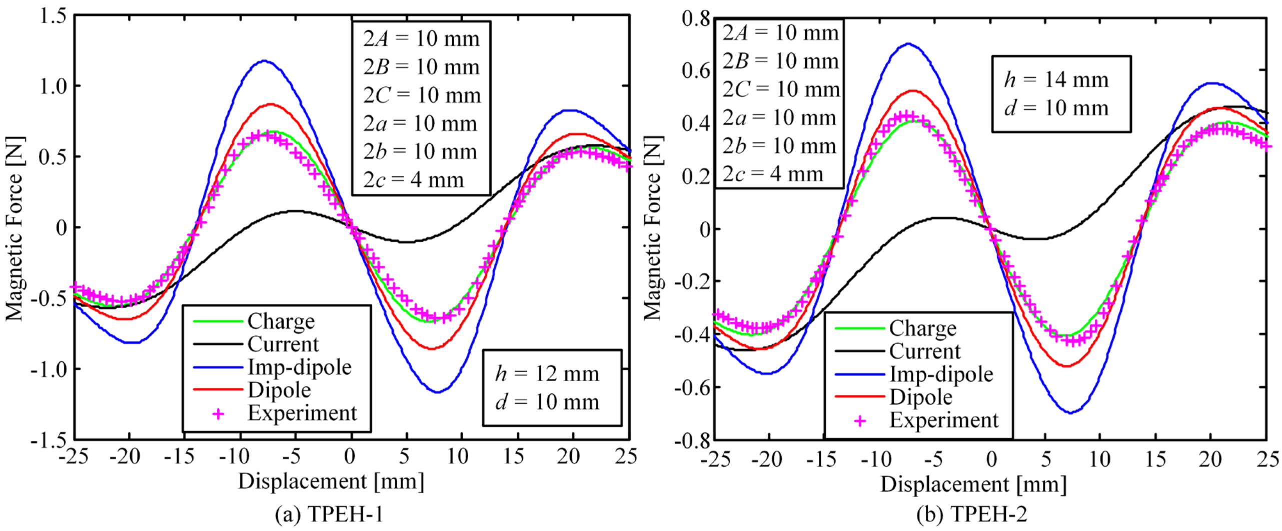


**Figure 12.** Experimental comparison for magnetic force of TPEH

Therefore, from the analysis of BPEH, the influence of $h$ on the magnetic force for all modeling methods can be in good agreement with the numerical investigation. With an increase of $h$, both the magnetic dipole method and improved dipole method can be the most accurate while the magnetic force calculated by the magnetic current method can have some deviation from the experimental result. As for the TPEH, during the increasing process of distance $h$, both magnetic dipole method and improved dipole method can match better with experimental result, but magnetic current method shows a higher error.

Since the nature frequency is a key factor to evaluate the dynamic response of energy harvester, there are two main methods used to obtain the natural frequency of linear cantilever beam. Firstly, it can be obtained by theoretical calculation of equivalent mass and equivalent stiffness according to the dimensions and the material properties of cantilever beam. Secondly, natural frequency can be identified from the frequency sweep or damped free vibration experiments. In addition to the equivalent mass and the equivalent stiffness, the damping factor and the electromechanical coupling factor are also important to affect the output performance of the system. The damping factor can be identified from the resonance amplification and damping ratio, while the electromechanical coupling factor can be obtained from the voltage response of linear system.

More importantly, since the difference between the linear and the multi-stable piezoelectric energy harvesters is the magnet, these parameters including equivalent mass, damping factor, equivalent stiffness and electromechanical coupling factor can be used to analyze the multi-stable piezoelectric energy harvester. From the application constraints of magnetic force modeling methods presented in this paper, the accurate magnetic force can be calculated by selecting the proper modeling methods to obtain desired nonlinear characteristics. The influence of the size, position, and rotational angle of permanent magnets on magnetic force can be investigated. Then, the frequency response of nonlinear multi-stable energy harvesters can be obtained by solving the governing equation through harmonic balance method or Runge-Kutta method. Therefore, the optimal structural parameters can be obtained to improve the performance of multi-stable energy harvesters.

## 5 Conclusion

The influence of structural parameters and magnets dimensions on the accuracy of the calculation of the magnetic force has been investigated among different modeling methods, including the magnetic dipole, improved dipole, magnetic current and magnetic charge methods. In addition, their relative accuracy and the application constraints for magnetic force calculation in multi-stable piezoelectric energy harvesters have been evaluated by both theoretical expression and numerical results. Consequently, experimental measurements are performed to demonstrate the applicability of these methods for bi-stable and tri-stable energy harvesters with a range of structural parameters. The applicability of these modeling methods can be concluded as follows:

(1) The improved dipole method is suitable for $\zeta \leq 0.4$, and an increase in $\zeta$ or decrease in $h$ can improve the error of this method. (2) The magnetic dipole method is preferable for a large $h$, where an increase in $h$ can allow magnets to be regarded as dipoles to improve accuracy. (3) The magnetic current method is favorable for conditions when the length along the $z$ direction is 6 mm or $h$ = 10 mm. The error of the magnetic current method can decrease with an increase in the length of the magnet along the $x$ direction or $y$ direction. (4) It is also interesting that when all dimensions of the magnet are the same, $2A = 2B = 2C$ = 10 mm or $2A = 2B = 2C$ = 8 mm, the magnetic dipole method can be more consistent with simulation result. (5) The magnetic force calculation by magnetic charge method is not limited to the application conditions, but this method has complicated expressions. These observations provide new insights into the selection of modelling methods for the design of nonlinear energy

harvesters.

## Acknowledgement

This study was supported by the National Natural Science Foundation of China (Grant No. 51975453), China Postdoctoral Science Foundation (2020M682336), Royal Society (Grant No. IEC\NSFC\170589).

## References

Abdelmoula H, Zimmerman S and Abdelkefi A (2017) Accurate modeling, comparative analysis, and performance enhancement of broadband piezoelectric energy harvesters with single and dual magnetic forces. *International Journal of Non-linear Mechanics* 95:355–363

Agashe JS and Arnold DP (2008) A study of scaling and geometry effects on the forces between cuboidal and cylindrical magnets using analytical force solutions. *Journal of Physics D* 41(10):105001

Akoun G and Yonnet JP (1984) 3D analytical calculation of the forces exerted between two cuboidal magnets. *IEEE Transactions on Magnetics* 20(5):1962–1964

Arrieta AF, Hagedorn P, Erturk A and Inman DJ (2010) A piezoelectric bistable plate for nonlinear broadband energy harvesting. *Applied Physics Letters* 97(10):104102

Barton DAW, Burrow SG and Clare LR (2010) Energy Harvesting From Vibrations With a Nonlinear Oscillator. *Journal of Vibration and Acoustics* 132(2):21009

Cao J, Zhou S, Wang W and Lin J (2015) Influence of potential well depth on nonlinear tristable energy harvesting. *Applied Physics Letters* 106(17):173903

Charpentier JF and Lemarquand G (1999) Optimal design of cylindrical air-gap synchronous permanent magnet couplings. *IEEE Transactions on Magnetics* 35(2):1037–1046

Cottone F, Vocca H and Gammaitoni L (2009) Nonlinear energy harvesting. *Physical Review Letters*

102(8):80601

Erturk A (2012) Assumed-modes modeling of piezoelectric energy harvesters: Euler-Bernoulli, Rayleigh, and Timoshenko models with axial deformations. *Computers & Structures* 106:214–227

Erturk A, Hoffmann J and Inman DJ (2009) A piezomagnetoelastic structure for broadband vibration energy harvesting. *Applied Physics Letters* 94(25):254102–254105

Fang S, Wang S, Miao G, Zhou S, Yang Z, Mei X and Liao WH (2020a) Comprehensive theoretical and experimental investigation of the rotational impact energy harvester with the centrifugal softening effect. *Nonlinear Dynamics* 101(1):123–152

Fang S, Wang S, Zhou S, Yang Z and Liao WH (2020b) Analytical and experimental investigation of the centrifugal softening and stiffening effects in rotational energy harvesting. *Journal of Sound and Vibration* 488:115643

Fang S, Wang S, Zhou S, Yang Z and Liao WH (2020c) Exploiting the advantages of the centrifugal softening effect in rotational impact energy harvesting. *Applied Physics Letters* 116(6):63903

Friswell MI, Ali SF, Bilgen O, Adhikari S, Lees AW and Litak G (2012) Non-linear piezoelectric vibration energy harvesting from a vertical cantilever beam with tip mass. *Journal of Intelligent Material Systems and Structures* 23(13):1505–1521

Fu H and Yeatman EM (2017) A methodology for low-speed broadband rotational energy harvesting using piezoelectric transduction and frequency up-conversion. *Energy* 125:152–161

Gammaitoni L, Neri I and Vocca H (2009) Nonlinear oscillators for vibration energy harvesting. *Applied Physics Letters* 94(16):164102

Gao Y, Leng Y, Javey A, Tan D, Liu J, Fan S and Lai Z (2016) Theoretical and applied research on bistable dual-piezoelectric-cantilever vibration energy harvesting toward realistic ambience. *Smart Materials and Structures* 25(11):115032

Li H, Qin W, Lan C, Deng W and Zhou Z (2016) Dynamics and coherence resonance of tri-stable energy harvesting system. *Smart Materials and Structures* 25(1):15001

Harne RL and Wang KW (2014) Prospects for Nonlinear Energy Harvesting Systems Designed Near the Elastic Stability Limit When Driven by Colored Noise. *Journal of Vibration and Acoustics* 136(2):21009

He Q and Daqaq MF (2016) Electric load optimization of a nonlinear mono-stable duffing harvester excited by white noise. *Meccanica* 51(5):1027–1039

He Q and Daqaq MF (2014) Influence of potential function asymmetries on the performance of nonlinear energy harvesters under white noise. *Journal of Sound and Vibration* 333(15):3479–3489

Kim P and Seok J (2014) A multi-stable energy harvester: Dynamic modeling and bifurcation analysis. *Journal of Sound and Vibration* 333(21):5525–5547

Koszewnik A, Ołdziej D and Amaro MB (2022) Parameter Optimization of a Magnetic Coupled Piezoelectric Energy Harvester with the Homogenized Material—Numerical Approach and Experimental Study. *Sensors* 22(11):4073.

Lai SK, Wang C and Zhang LH (2019) A nonlinear multi-stable piezomagnetoelastic harvester array for low-intensity, low-frequency, and broadband vibrations. *Mechanical Systems and Signal Processing* 122:87–102

Leland ES and Wright PK (2006) Resonance tuning of piezoelectric vibration energy scavenging generators using compressive axial preload. *Smart Materials and Structures* 15(5):1413–1420

Leng Y, Tan D, Liu J, Zhang Y and Fan S (2017) Magnetic force analysis and performance of a tri-stable piezoelectric energy harvester under random excitation. *Journal of Sound and Vibration* 406:146–160

Litak G, Friswell MI and Adhikari S (2010) Magnetopiezoelastic energy harvesting driven by random excitations. *Applied Physics Letters* 96(21):214103

Masana R and Daqaq MF (2011) Relative performance of a vibratory energy harvester in mono- and bi-stable potentials. *Journal of Sound and Vibration* 330(24):6036–6052

Moon FC and Holmes PJ (1979) A magnetoelastic strange attractor. *Journal of Sound and Vibration* 65(2):275–296

Rezaei M and Talebitooti R (2022) Investigating the performance of tri-stable magneto-piezoelastic absorber in simultaneous energy harvesting and vibration isolation. *Applied Mathematical Modelling* 102:661–693.

Rezaei M, Talebitooti R and Liao WH (2021) Exploiting bi-stable magneto-piezoelastic absorber for simultaneous energy harvesting and vibration mitigation. *International Journal of Mechanical Sciences* 207:106618.

Rezaei M, Talebitooti R and Liao WH (2022) Investigations on magnetic bistable PZT-based absorber for concurrent energy harvesting and vibration mitigation: Numerical and analytical approaches. *Energy* 239:122376.

Stanton SC, McGehee CC and Mann BP (2009) Reversible hysteresis for broadband magnetopiezoelastic energy harvesting. *Applied Physics Letters* 95(17):174103

Stanton SC, McGehee CC and Mann BP (2010) Nonlinear dynamics for broadband energy harvesting: Investigation of a bistable piezoelectric inertial generator. *Physica D: Nonlinear Phenomena* 239(10):640–653

Tang L and Yang Y (2012) A nonlinear piezoelectric energy harvester with magnetic oscillator. *Applied*

*Physics Letters* 101(9):94102

Upadrashta D and Yang Y (2015) Finite element modeling of nonlinear piezoelectric energy harvesters with magnetic interaction. *Smart Materials and Structures* 24(4):45042

Wang C, Zhang Q, Wang W and Feng J (2018a) A low-frequency, wideband quad-stable energy harvester using combined nonlinearity and frequency up-conversion by cantilever-surface contact. *Mechanical Systems and Signal Processing* 112:305–318

Wang G, Liao WH, Zhao Z, Tan J, Cui S, Wu H and Wang W (2019) Nonlinear magnetic force and dynamic characteristics of a tri-stable piezoelectric energy harvester. *Nonlinear Dynamics* 97(4):2371–2397

Wang G, Wu H, Liao WH, Cui S, Zhao Z and Tan J (2020) A modified magnetic force model and experimental validation of a tri-stable piezoelectric energy harvester. *Journal of Intelligent Material Systems and Structures* 31(7):967–979

Wang W, Cao J, Bowen CR, Zhang Y and Lin J (2018b) Nonlinear dynamics and performance enhancement of asymmetric potential bistable energy harvesters. *Nonlinear Dynamics* 94(2):1183–1194

Yang Z, Zhou S, Zu J and Inman D (2018) High-Performance Piezoelectric Energy Harvesters and Their Applications. *Joule* 2(4):642–697

Yung KW, Landecker PB and Villani DD (1998) An Analytic Solution for the Force Between Two Magnetic Dipoles. *Physical Separation in Science and Engineering* 9(1):39–52

Zhang Y, Cao J, Wang W and Liao WH (2021) Enhanced Modeling of Nonlinear Restoring Force in Multi-Stable Energy Harvesters. *Journal of Sound and Vibration* 494:115890

Zhao LC, Zou HX, Gao QH, Yan G, Liu FR, Tan T, Wei KX and Zhang WM (2019a) Magnetically modulated orbit for human motion energy harvesting. *Applied Physics Letters* 115(26):263902

Zhao LC, Zou HX, Yan G, Liu FR, Tan T, Zhang WM, Peng ZK and Meng G (2019b) A water-proof magnetically coupled piezoelectric-electromagnetic hybrid wind energy harvester. *Applied Energy* 239:735–746

Zhao LC, Zou HX, Yan G, Zhang WM, Peng ZK and Meng G (2018) Arbitrary-directional broadband vibration energy harvesting using magnetically coupled flextensional transducers. Smart *Materials and Structures* 27(9):95010

Zhou S, Cao J, Erturk A and Lin J (2013) Enhanced broadband piezoelectric energy harvesting using rotatable magnets. *Applied Physics Letters* 102(17):173901

Zhou S, Cao J, Inman DJ, Lin J, Liu S and Wang Z (2014) Broadband tristable energy harvester: Modeling and experiment verification. *Applied Energy* 133:33–39

Zou HX, Zhang WM, Li WB, Hu KM, Wei KX, Peng ZK and Meng G (2017) A broadband compressive-mode vibration energy harvester enhanced by magnetic force intervention approach. *Applied Physics Letters* 110(16):163904